ELSEVIER

Earth and Planetary Science Letters 193 (2001) 227–236

EPSL

www.elsevier.com/locate/epsl

# A low viscosity wedge in subduction zones

Magali I. Billen *, Michael Gurnis

*Seismological Laboratory, California Institute of Technology, Pasadena, CA 91125, USA*

Received 22 May 2001; received in revised form 14 August 2001; accepted 20 August 2001

**Abstract**

Geochemical, petrologic and seismological observations indicate that there may be high concentrations of water in the region above a subducting slab (the mantle wedge), which could decrease the viscosity of the mantle locally by several orders of magnitude. Using numerical models we demonstrate that a low viscosity wedge has a dramatic influence on the force balance in a subduction zone and leads to an observable signal in the topography, gravity and geoid. A regional dynamic model of the Tonga–Kermadec subduction zone shows that the viscosity of the wedge is at least a factor of 10 smaller than surrounding mantle lithosphere and asthenosphere, consistent with estimates from seismic dissipation and deformation experiments. 

*Keywords:* subduction zones; viscosity; gravity anomalies; topography; Tonga Trench; Kermadec Trench

## 1. Introduction

The mantle wedge is the region of the mantle lithosphere and asthenosphere that lies above a subducting oceanic plate and beneath the overriding plate in a convergent margin. The wedge plays an important role in subduction zone processes: the viscosity ($\eta$) of the wedge links the negative buoyancy force of the sinking slab to the surface, while melt generation in the wedge links the input of volatiles from the slab [1] to magma extruded at the island-arc and back-arc spreading center. However, these dynamic and geochemical/petrologic processes in the wedge do not act independently: the viscosity of the wedge, which affects the dynamics, depends on the presence of volatiles and melt, the temperature distribution (which itself depends on melting) and the deformation mechanism [2].

Subduction dynamics depend on the buoyancy of the subducting plate, the viscosity structure of the mantle, and coupling between the subducting and overriding plate. The location and morphology of the subducted lithosphere, delineated by deep seismicity [3] and tomographic images [4], constrains the buoyancy of the slab, while the viscosity structure is constrained by surface observations. For example, observations sensitive to the viscosity structure include: (a) geoid and gravity anomalies (Fig. 1A), which have a long wavelength high and short wavelength low directly over subduction zones [5,6] and (b) topography (Fig. 1C), characterized by the morphology and depth of the trench, the presence (or lack) of a forebulge and high or low topography on the

* Corresponding author. Fax: +1-626-564-0715.
*E-mail address:* magali@gps.caltech.edu (M.I. Billen).

0012-821X/01/$ – see front matter 
PII: S0012-821X(01)00482-4

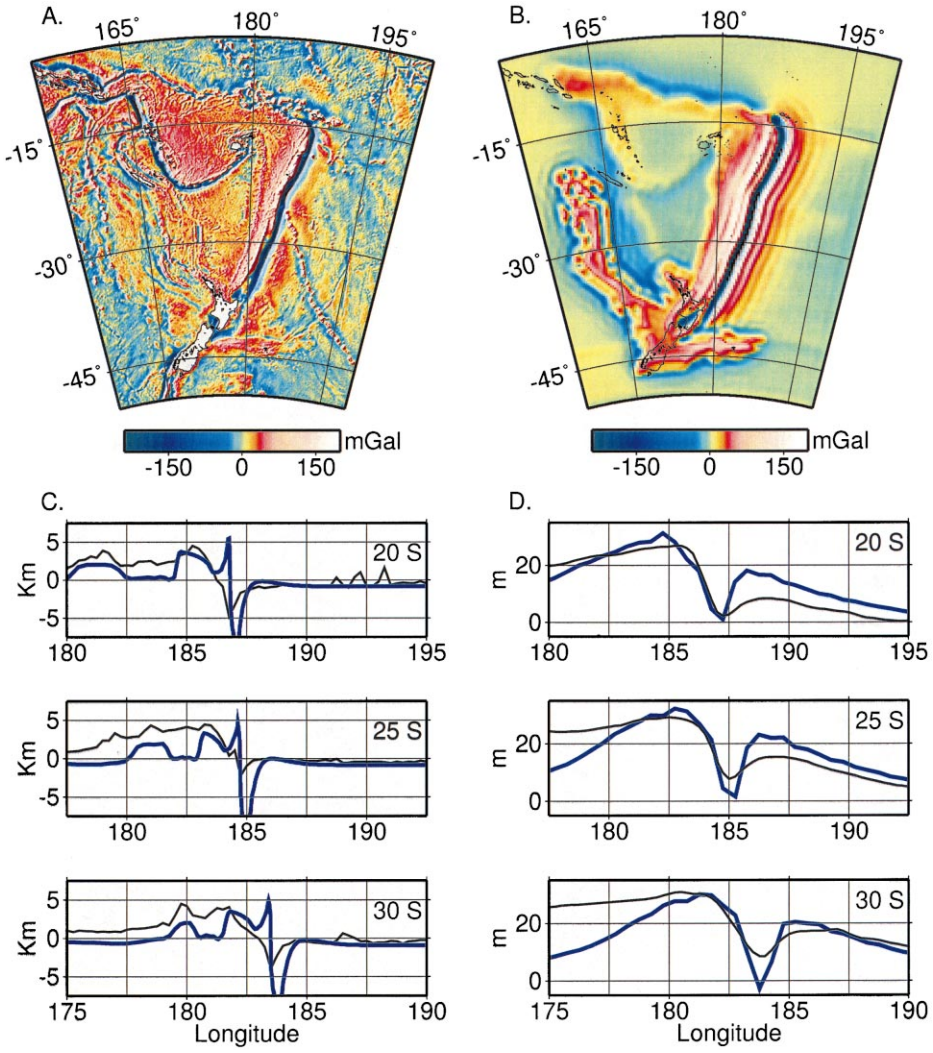


Fig. 1. (A) Free-air gravity anomaly from satellite altimetry [41] for the Tonga–Kermadec region. (B) Free-air gravity anomaly for 3D dynamic model including a low viscosity region in the wedge. (C) Comparison of topography along east–west profiles across the subduction zone at 20, 25 and 30°S (thick/blue) to observed topography (thin/black) [42]. Model topography has an arbitrary reference height (here set to zero) therefore, observed topography is adjusted to equal zero at the model boundary. (D) Comparison of model geoid anomalies (thick/blue) with observed (thin/black) [43] along east–west profiles. An east–west linear ramp is removed from each of the observed and model geoid profiles so that the geoid equals zero at the model boundaries.

overriding plate [7]. Surface observables over subduction zones vary over several scales and therefore the physics required to explain these features is complex.

Previous analytic and numerical models fail to adequately reproduce the multiscale characteristic of subduction zone surface observables such as topography and geoid. For example, thin elastic plate models for the subducting plate match gross trench morphology and short wavelength gravity [7], but are not dynamic given that the forces driving deformation are not considered. Dynamic models, which include a radial viscosity structure, match the long wavelength geoid ($>1000$ km) using analytic solutions of viscous flow [8], but observed shorter wavelength geoid features are

not predicted. Dynamic, numerical models of subduction which include a fault interface in the lithosphere along the plate boundary, successfully reproduce two-dimensional (2D) trench topography [9–11] and match the long wavelength geoid anomaly in 2D and 3D regional models [11,12]. However, contrary to observations, these numerical models predict large (3–4 km), negative dynamic topography on the overriding plate (in the arc/back-arc region). Such an excessively deep back-arc basin in the models creates a broad ($\sim$500 km) depression in the gravity and geoid anomalies over the back-arc, that is not observed in active subduction zones. Down-warping of the overriding plate in subduction zone models is a direct consequence of the dynamic coupling of the negative buoyancy force of the slab to the overriding lithosphere through the wedge.

Geochemical and petrologic data indicate that fluids from the subducting slab are incorporated into the wedge prior to melting to form island-arc magmas [1,13,14]. Seismic studies in subduction zones reveal anomalies of low velocity [15,16] and high attenuation [16,17] in the wedge that suggest the presence of volatiles, particularly water [18] and possibly melt. While melting of the slab itself may occur in limited cases as suggested by the presence of high Mg# andesites (adakites) which include a component derived from partial melting of subducted slab [19], hydration of the mantle and lowering of the solidus are likely the more common cause for the seismic anomalies observed in the wedge and back-arc volcanism. The majority of well-defined quantitative experimental studies on rheology have been conducted at low pressures ($<$300 MPa, e.g. [20]). These studies have shown that plastic deformation of upper mantle minerals, particularly olivine, is significantly enhanced by the presence of water. Rheology of minerals at higher pressures is still poorly constrained. However, a recent study on olivine at pressures up to 2 GPa has established a quantitative flow law for olivine that can be extrapolated to higher pressure conditions [21]. This work combined with the results of Kohlstedt et al. [22] suggests that at higher water fugacity conditions likely in the deep upper mantle in subduction zones, weakening effects of water will be much more pronounced. These observations and experiments suggest the viscosity in the region above a subducting slab may be substantially less than the background asthenosphere and mantle lithosphere. Such a low viscosity wedge (LVW) could affect the flow, force balance and surface deformation in a subduction zone, as well as processes governing the transport of fluids and generation of melt.

## 2. Dynamic models with a LVW

We investigate the influence of a LVW on the dynamics of a subduction zone, using a finite element model for instantaneous viscous flow. Stokes flow calculations are solved using CitcomT [23], a 3D, spherical finite element code, based on the cartesian code CITCOM [12]. The momentum and continuity equations are solved with a primitive variable formulation and validated with known analytic solutions with large radial and lateral variations in viscosity [24]. The top and bottom surfaces have free slip, isothermal boundary conditions, while the side-walls have reflecting boundary conditions. A fault (shear zone) is included along the subduction zone plate boundary in the upper 100 km. The fault is modeled with boundary conditions allowing for continuous normal stress and discontinuous tangential stress on the fault surface [9,10]. The presence of the fault is required for a trench to form at the plate boundary. However, the fault discontinuity creates a stress singularity at the fault tip. This stress singularity leads to unconstrained maximum trench depth and fore-arc height. Therefore, a yield stress, $\sigma_y = 75$ MPa, is used in the upper 100 km to constrain the stress near the fault tip. In addition, when calculating the gravity the maximum trench depth and fore-arc height are truncated at 5 km.

The model domain extends from the surface to the core–mantle boundary and extends 45° in both longitude and latitude for 3D models. 2D models are taken from an east–west cross section through the 3D models at 28°S. The buoyancy structure (Fig. 2A) of the slab down to 660 km and the location of the fault interface in the top

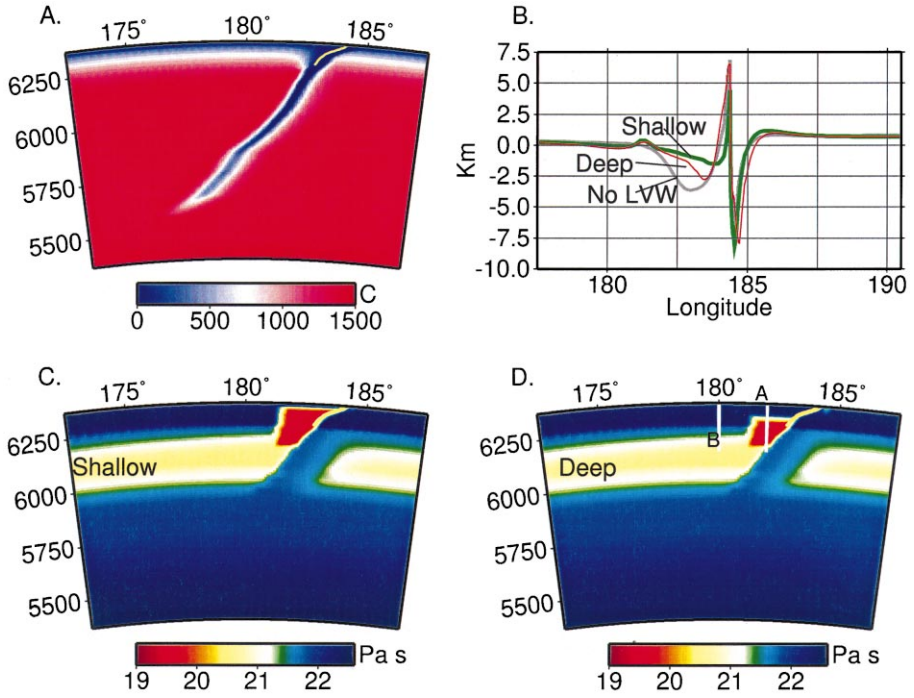


Fig. 2. (A) Temperature profile from 3D model at 28°S used in 2D models with uniform lithosphere thickness shown for a 15° region spanning the subduction zone. (B) Comparison of dynamic topography with a deep (thin/red) and shallow (thick/green) LVW and without a LVW (gray). Background radial, temperature-dependent viscosity structure with superimposed large, shallow LVW (C) and a small, deep LVW (D). Vertical white lines, labeled A and B, indicate boundaries of other LVW's investigated (see text). Yellow line is the location of the fault interface.

100 km are constrained to match the location of seismicity which extends from the surface to a maximum depth of 660 km (Fig. 2A). The true dip of the fault at the surface ranges from 10 to 30°. However, due to numerical constraints on the allowed distortion of the elements, the minimum dip of the fault in the upper 10 km is 30°.

The imposed temperature structure is obtained by first creating a steady-state temperature model. We solve the advection–diffusion equation for 45 million years of subduction starting with 50 Myr old lithosphere [25]. Flow velocities are specified to follow the location of seismicity over a zone of 100 km thickness (the slab) and an approximate (due to varying dip of the slab) corner flow velocity solution above and below the slab. The background radial viscosity structure is temperature-dependent with Newtonian viscosity. The maximum viscosity of the lithosphere and lower mantle is $3\times10^{22}$ Pa s and the minimum viscosity of the asthenosphere is $3\times10^{20}$ Pa s. Viscosity of the slab depends on temperature and has a maximum value of $3.0\times10^{21}$ Pa s for the coldest regions.

Initially, 2D models are used to explore the general influence of a LVW on the flow field, dynamic topography and trade-offs between the shape of the viscosity region and magnitude of the viscosity reduction. 3D models for the Tonga–Kermadec subduction zone are then used to test whether including a LVW greatly improves model agreement with observations of topography, gravity and geoid.

### 2.1. 2D models

Including a low viscosity region in the wedge dramatically changes the dynamic topography (Fig. 2B). Comparison of 2D models with and without a LVW (Fig. 2C,D) demonstrates that a LVW with a viscosity 10 times smaller than the

asthenosphere viscosity, reduces the down-warping of the overriding plate from a broad depression of more than 4 km deep (equivalent model without LVW) to a narrow depression of less than 2.5 km (Fig. 2B). In addition, the trench is deeper and the forebulge on the subducting plate is more pronounced with the LVW. Reduction of the overriding plate topography depends on the depth and overall extent of the LVW. A shallow, large LVW (Fig. 2C) decreases the magnitude and lateral extent of the down-warping more than a smaller and deeper LVW (Fig. 2D). Decreasing the viscosity of the wedge further (by a factor of 100 or 1000) has little effect on the topography but does influence the pattern and magnitude of flow in the wedge. We will return to this point in Section 3.

The reason for the change in topography and flow is clarified by examining the change in the pressure due to the LVW. For a model without a LVW, the dynamic pressure, $P$, from the top of the slab at 200 km depth to the surface is low (Fig. 3A), indicating suction into this region (high pressure indicates expansion). Low pressure creates a downward stress on the surface and negative dynamic topography. For a model with a LVW, the pressure is higher in the wedge, increasing significantly above the LVW, except for a region very close to the trench (Fig. 3B). This difference in the pressure above the slab is also responsible for increasing the trench depth and creating the forebulge. The low pressure (suction) above the slab acts to pull the slab up supporting part of the negative buoyancy of the slab and reducing the net downward force on the slab [26,27]. When the LVW is added there is less suction above the slab acting to pull the slab up and the coupling of the slab to the wedge is reduced because the viscosity in the wedge is lower. These two effects act to deepen the trench due to the larger net downward force on the subducting plate and increase the forebulge height by increasing the viscous bending stresses within the lithosphere, outboard of the fault.

A uniform reduction of the asthenosphere viscosity does not have the same outcome as reduc-

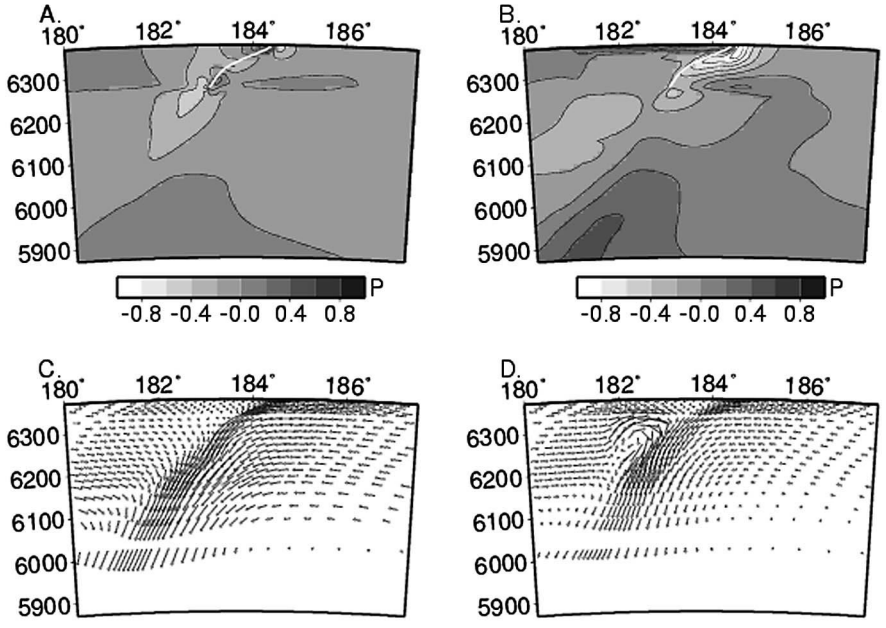


Fig. 3. Dynamic pressure, $P$, normalized by the maximum for (A) model without a LVW ($P_{max} = 1.57 \times 10^8$ N/m$^2$) and (B) model with a shallow LVW ($P_{max} = 0.96 \times 10^8$ N/m$^2$). Contour interval is 0.2. Flow field (velocity, $v$) for (C) model without a LVW ($v_{max} = 1.5$ cm/yr) and (D) model with a shallow LVW ($v_{max} = 4.8$ cm/yr). White line is the location of the fault interface.

ing the viscosity within an isolated region of the wedge. The limited extent of the LVW modifies the long and short wavelength pattern of flow. In the model without a LVW, flow in the mantle and lithosphere is dominated by the sinking motion of the slab and is long wavelength in character (Fig. 3C). The presence of the LVW interrupts the long wavelength character of the flow and creates a stronger component of horizontal flow entering the wedge and upward flow in the wedge (Fig. 3D). The horizontal extent of the LVW is also important. A narrower LVW, extending only to boundary A (Fig. 2D), allows the slab flow to couple to the surface beyond the low viscosity region resulting in a topography depression to the left of the boundary. While a wider region extending to boundary B (Fig. 2D) also reduces the amplitude of the depression (to $\sim$2.5 km), the long wavelength character of the flow again dominates so that this depression extends over the full extent of the LVW rather than being isolated to a narrower region near the trench.

In addition to the models presented in Figs. 2 and 3, other models were used to investigate the effect of the dimensions and placement of the LVW. As presented above, the width and depth to the top of the LVW have the largest influence on the topography. The maximum depth of the LVW has little effect on the topography, but does influence the flow. Extending the maximum depth of LVW for a wide region (200 km wide) creates a stronger upward component of flow within the wedge.

### 2.2. 3D models: Tonga–Kermadec subduction zone

We have further tested whether such a LVW is consistent with geophysical observations by comparing predictions of dynamic topography, gravity and geoid for 3D regional models of the Tonga–Kermadec subduction zone, including a LVW ($\eta_{\mathrm{lvw}} = 3 \times 10^{19}$ Pa s). We include realistic variations in the density structure of the lithosphere due to age [28–30] and crustal thickness [31]. Fig. 1 shows a comparison of observed free-air gravity (Fig. 1A) with the model prediction (Fig. 1B) and comparisons of topography (Fig. 1C) and geoid (Fig. 1D) for three east–west profiles across the trench. The topography profiles agree well with the observations over the back-arc and the shape of the trench, although the maximum depth of the trench and height of the fore-arc and forebulge are still larger than observed.

While the applied yield stress does reduce the trench and fore-arc topography, the remaining excess topography may be due to remaining stress near the fault. The yield stress of 75 MPa was chosen to limit the region affected by the yield stress to the immediate region of the fault. A lower yield stress would be more effective at reducing the stress and the topography near the fault, but would also lead to a broad region of weakening on the subducting plate that causes the trench to widen. The stresses in the model depend linearly on the density anomaly of the slab. The maximum density anomaly in the slab of 80 kg/m$^3$ (due to the temperature anomaly) occurs in the upper 200 km of the slab. If the density anomaly of the slab is lower than assumed here (possibly due to a lower coefficient of thermal expansion or phase changes), then the stresses would also be lower leading to a smaller trench, fore-arc and forebulge. The steeper dip of the fault at the surface in the models (30°) than observed (10–15°) may also contribute to the forebulge topography. The steeper dip of fault in the models (required by limitations on the maximum allowed distortion of elements within the mesh) creates a small region of horizontal compression in the subducting plate that may add to the forebulge height.

The model reproduces the observed long wavelength positive geoid and gravity high with a single short wavelength depression over the trench. It is important to note that in order to achieve good agreement between both the topography and the geoid it is necessary to include both the variations in plate age and crustal thickness in addition to the low viscosity region in the wedge. Models which include only variations in plate age and/or crustal thickness variations are still dominated by the long wavelength depression in the back-arc region making it difficult to match the long wavelength geoid and gravity. Models which do not include both lithospheric age and crustal thickness variations do not agree with the observed topography and short wavelength gravity.

## 3. Discussion

The 2D models demonstrate that the geometry of the LVW is important and that neither a simple reduction of the viscosity throughout the asthenosphere nor a change in the wedge viscosity from 10 to 100 times smaller than the asthenosphere viscosity substantially influence the topography. Instead, in both these cases, we find that the velocity increases but the pressure remains the same. This is the result of a balance of forces in which the driving force (i.e. the buoyancy of the slab) is fixed and is balanced by viscous coupling within the asthenosphere controlling slab descent. In this case, any reduction in viscosity is matched by an increase in velocity to balance the driving force, keeping the pressure and resulting topography constant. However, one can imagine several cases in which the slab descent is not controlled by the asthenosphere viscosity: (1) if the velocity of the plates are controlled by the strength of the oceanic lithosphere as it descends into the mantle [35]; and (2) if the slab is strong and coupled to a higher viscosity lower mantle, so that slab rate is controlled by the viscosity of the lower mantle [12]. In these two cases, flow in the wedge becomes analogous to the kinematically driven cornerflow. The velocity of the slab, $U_{\mathrm{slab}}$, in a cornerflow is a boundary condition which does not depend on the wedge viscosity, $\eta_{\mathrm{w}}$, and the pressure in the wedge is $P \propto -\eta_{\mathrm{w}} U_{\mathrm{slab}}$. In this case, since the velocity is fixed, any reduction in the wedge viscosity reduces the magnitude of the pressure and the basin topography on the overriding plate. However, even in this case, the shape of the wedge becomes important. In a cornerflow, while the velocity in the wedge is proportional to the boundary velocity and pressure is proportional to the viscosity, the pattern or distribution of velocity and pressure remain the same. Therefore, the only way to change the character of the flow in the wedge is to modify the geometry of the wedge, as we have by introducing a shallow LVW.

### 3.1. Mineral physics constraints on wedge viscosity

Estimates of viscosity in the wedge depend on observed seismic wave anomalies and attenuation, and theoretical and experimentally determined relationships between these observations and subsolidus creep. Experiments show that both attenuation and steady-state creep have similar activation energy and are similarly affected by water. Both attenuation, $Q^{-1}$, and viscosity, $\eta$, have an exponential dependence on temperature:

$$Q^{-1} \sim \omega^{-\alpha} \exp\left(\frac{-\alpha H^*}{R T_{\mathrm{eff}}}\right) \tag{1}$$

and

$$\eta \sim \eta_0 \exp\left(\frac{H^*}{R T_{\mathrm{eff}}}\right) \tag{2}$$

where $H^*$ is activation enthalpy, $T_{\mathrm{eff}}$ is the rheologically effective temperature which incorporates the effects of water, $\omega$ is frequency and $\alpha$ is a constant [32]. Karato [33] hypothesizes that the kinetics of both attenuation and steady-state creep are affected by water through the same mechanism. Therefore, attenuation and viscosity can be related by combining Eqs. 1 and 2 [33]:

$$\eta / \eta_0 = (Q/Q_0)^{(1/\alpha)} \tag{3}$$

where $\alpha = 0.23$, is determined from both seismological and experimental data [32] and $Q_0$ is the reference attenuation. Using observations of low $Q$ for P waves in the wedge of the Tonga–Kermadec subduction zone of $Q = 70$–$150$ [17] and a reference attenuation for P waves in the asthenosphere of $Q_0 = 200$ [34], Eq. 3 predicts the viscosity of the wedge should range from 0.01 to 0.28 times the reference viscosity. While Eq. 3 provides a simple relation between attenuation and viscosity, seismic velocity anomalies are better resolved than attenuation. P-wave anomalies in the wedge in the Tonga region range from $-2$ to $-6\%$ [4]. A more robust estimate of the viscosity variation based on seismic velocity ([33], Fig. 5) predicts a similar reduction in the wedge viscosity of $2 \times 10^{-2}$ for a P wave anomaly of $-2\%$ and a much larger reduction of $8 \times 10^{-4}$ for a P wave anomaly of $-5\%$. Therefore, the independent estimate of the minimum viscosity reduction in the

wedge, of at least a factor of 10, from our dynamic models is well within the range of viscosity variation predicted by mineral physics and seismic observations. This agreement between independent estimates of the wedge viscosity supports our hypothesis of a weak mantle wedge.

### 3.2. Geophysical and geochemical implications of a LVW

#### 3.2.1. Fluids in the wedge

The presence of a LVW has important implications for interpreting geochemical and petrologic observations that constrain the thermal and chemical state of the wedge. The viscosity structure strongly influences the pressure field, which couples flow of fluids to the solid flow in the wedge. Timescales for fluids traveling through the slab–wedge system range from several million years to as short as 30 000 yrs [36]. Therefore, the effect of the LVW on the path fluids take to the surface could provide important constraints on the depths at which fluids are leaving the slab and migrating through the wedge.

#### 3.2.2. Time-dependent structure of the wedge

The viscosity of the wedge also has an obvious effect on the pattern of flow in the wedge, causing material to be drawn up into the wedge corner (Fig. 3D). In time-dependent models this flow could draw deep, hotter material into the wedge. Melting experiments on arc basalt compositions require that temperatures in the wedge be $\sim$1400°C at 100 km depth [14]. This is far warmer than $\sim$1000°C temperature at the same depth predicted by steady-state, kinematic temperature models that use an imposed flow velocity field for an isoviscous asthenosphere [37]. Since the pattern of flow in dynamic models depends on the relative magnitude of the viscosity reduction in the wedge, the temperature structure from time-dependent dynamic models including a LVW would serve as an additional constraint on the wedge viscosity. However, it is not clear whether a LVW would be a stable feature. Davies and Stevenson [38] found that a localized source of buoyancy could modify the wedge flow to include a small-scale convection cell within the wedge. They suggest that such a reversal of flow would lead to cooling of the wedge and reduction of the buoyancy force creating a non-steady-state modification of the wedge flow and temperature structure. While cooling of the wedge would increase viscosity, the influence of water and melt may still be sufficient to maintain the LVW. Also, if only a modest reduction of viscosity occurs (10–100 times smaller), a local reversal of flow may not occur.

If the LVW is an unstable feature of subduction zones, the slab dip and coupling to the surface will change with time. This would lead to episodes of shallow or steeply dipping subduction and raising and lowering of the overriding plate. This type of behavior may be recorded in the history of basin development and sediment deposition on overriding continental plates [39,40], island-arc volcanics and present day morphology of slabs. One might expect a prominent basin to form early on during subduction before a substantial amount of slab dehydration has occurred and could affect the wedge viscosity. Similarly, the coupling between the slab and the surface might increase after prolonged periods of subduction, due to high integrated extents of melting of the wedge, making the wedge more refractory with a higher effective viscosity.

## 4. Conclusions

Using dynamic models of Stokes flow we have shown that an isolated low viscosity region in the wedge influences the pressure field and pattern and vigor of flow within the wedge and slab, which in turn affects topography and gravity. Improved agreement between models that include a LVW and observations of topography and geoid provides a constraint on the minimum viscosity contrast between the wedge and asthenosphere of at least a factor of 10. The maximum influence of the LVW is achieved for shallow (20 km) and broad low viscosity regions that are at least as wide as the deep basin topography present in the models without a LVW. The maximum depth of the LVW has little influence on the topography for depths exceeding 100 km, but does influence pattern of flow in the wedge. Larger reductions in

the viscosity of the wedge do not further reduce the topography, but instead modify the flow pattern and lead to larger velocities within the wedge. Time-dependent models are needed to constrain the maximum viscosity contrast permitted in the wedge and to investigate the effect of a LVW on the evolution of the slab–wedge system.

## Acknowledgements

We thank J. Huw Davies, D. Bercovici and an anonymous reviewer for their reviews, D. Anderson, J. Eiler, L. Lavier, and M. Simons for constructive comments on the manuscript and Shun Karato for helpful discussion of experimental data on attenuation and viscosity. Calculations were carried out on the facilities of the Caltech Center for Advanced Computer Research (CACR). Supported by NSF grants EAR-9725629 and EAR-9814577, Contribution No. 8805, Division of Geological and Planetary Sciences, California Institute of Technology.*[SK]*

## References

[1] J.D. Morris, W.P. Leeman, F. Tera, The subducted component in island arc lavas: constraints from Be isotopes and B–Be systematics, Nature 344 (1990) 31–36.
[2] G. Hirth, D.L. Kohlstedt, Water in the oceanic upper mantle: implications for rheology, melt extraction and the evolution of the lithosphere, Earth Planet. Sci. Lett. 144 (1996) 93–108.
[3] M.W. Hamburger, B.L. Isacks, Deep earthquakes in the Southwest Pacific: morphology and tectonic history, Earthq. Notes 55 (1985) 32.
[4] D. Zhao, Y. Xu, D.A. Wiens, L. Dorman, J. Hildebrand, S. Webb, Depth extent of the Lau back-arc spreading center and its relation to subduction processes, Science 278 (1997) 254–257.
[5] W.M. Kaula, Global gravity and tectonics, in: E.C. Robertson, J.F. Hays, L. Knopoff (Eds.), The Nature of the Solid Earth, McGraw-Hill, New York, 1972, pp. 385–405.
[6] A.B. Watts, M. Talwani, Gravity anomalies seaward of deep-sea trenches and their tectonic implications, Geophys. J.R. Astron. Soc. 36 (1974) 57–90.
[7] J.H. Bodine, A.B. Watts, On lithospheric flexure seaward of the Bonin and Mariana Trenches, Earth Planet. Sci. Lett. 43 (1979) 132–148.
[8] B.H. Hager, Subducted slabs and the geoid: constraints on mantle rheology and flow, J. Geophys. Res. 89 (B7) (1984) 6003–6015.
[9] S. Zhong, M. Gurnis, Controls on trench topography from dynamic models of subducted slabs, J. Geophys. Res. 99 (B8) (1994) 15683–15695.
[10] S. Zhong, M. Gurnis, L. Moresi, Role of faults, nonlinear rheology, and viscosity structure in generating plates from instantaneous mantle flow models, J. Geophys. Res. 103 (B7) (1998) 15255–15268.
[11] S. Zhong, M. Gurnis, Viscous flow model of a subduction zone with a faulted lithosphere: long and short wavelength topography, gravity and geoid, Geophys. Res. Lett. 19 (18) (1992) 1891–1894.
[12] L. Moresi, M. Gurnis, Constraints on the lateral strength of slabs from three-dimensional dynamic flow models, Earth Planet. Sci. Lett. 138 (1996) 15–28.
[13] J.M. Brenan, H.F. Shaw, F.J. Ryerson, Experimental evidence for the origin of lead enrichment in convergent-margin magmas, Nature 378 (1995) 54–57.
[14] Y. Tatsumi, M. Sakayuma, H. Fukuyama, I. Kushiro, Generation of arc basalt magmas and thermal structure of the mantle wedge in subduction zones, J. Geophys. Res. 88 (1983) 5815–5825.
[15] A. Hasegawa, D. Zhao, S. Hori, A. Yamamoto, S. Horiuchi, Deep structure of the Northeastern Japan Arc and its relationship to seismic and volcanic activity, Nature 352 (1991) 683–689.
[16] E. Roth, D. Wiens, D. Zhao, An empirical relationship between seismic attenuation and velocity anomalies in the upper mantle, Geophys. Res. Lett. 27 (2000) 601–604.
[17] M. Barazangi, B. Isacks, Lateral variations of seismic-wave attenuation in the upper mantle above the inclined earthquake zone of the Tonga Island Arc: deep anomaly in the upper mantle, J. Geophys. Res. 76 (1971) 8493–8515.
[18] S. Karato, H. Jung, Water, partial melting and the origin of the seismic low velocity and high attenuation zone in the upper mantle, Earth Planet. Sci. Lett. 157 (1998) 193–207.
[19] G.M. Yogodzinski, R.W. Kay, O.N. Volynets, A.V. Koloskov, S.M. Kay, Magnesian andesite in the Western Aleutian Komandorsky region: implications for slab melting and processes in the mantle wedge, J. Geophys. Res. 107 (1995) 505–519.
[20] S. Karato, M.S. Paterson, J.D. Fitzgerald, Rheology of synthetic olivine aggregates: influence of grain size and water, J. Geophys. Res. 91 (1986) 8151–8176.
[21] S. Karato, H. Jung, Effects of pressure on high-temperature dislocation creep in olivine, Philos. Mag. Ann. (2001), in press.
[22] D.L. Kohlstedt, H. Keppler, D.C. Rubie, Solubility of water in a, b, and g phases of $(Mg,Fe)_2SiO_4$, Contrib. Mineral. Petrol. 123 (1995) 345–357.
[23] M.I. Billen, M. Gurnis, Multiscale dynamic models of the Tonga–Kermadec subduction zone, Geophys. J. Int. (2001), in preparation.

[24] S. Zhong, Analytic solutions for Stokes' flow with lateral variations in viscosity, Geophys. J. Int. 124 (1996) 18–28.
[25] J.P. Eissen, A.J. Crawford, J. Cotten, S. Mettre, H. Bellon, M. Delaune, Geochemistry and tectonic significance of basalts in the Poya Terrane, New Caledonia, Tectonophysics 284 (1998) 203–219.
[26] D.J. Stevenson, J.S. Turner, Angle of subduction, Nature 270 (1977) 334–336.
[27] A. Tovish, G. Schubert, B.P. Luyendyk, Mantle flow pressure and the angle of subduction: non-Newtonian corner flows, J. Geophys. Res. 83 (1978) 5892–5898.
[28] R.D. Müller, W.R. Roest, J.Y. Royer, L.M. Gahagan, J.G. Sclater, Digital isochrons of the world's ocean floor, J. Geophys. Res. 102 (1997) 3211–3214.
[29] L.W. Kroenke, Cenozoic Tectonic Development of the Southwest Pacific, UN ESCAP CCOP/SOPAC Tech. Bull. 6, New Zealand, 1984.
[30] M.I. Billen, J. Stock, Origin and morphology of the Osbourn Trough, J. Geophys. Res. 105 (2000) 13481–13489.
[31] R.W. Raitt, R.L. Fisher, R.G. Mason, Tonga trench, in: Crust of the Earth, Geol. Soc. Am. Spec. Pap. 62 (1955) 237–254.
[32] S. Karato, H.A. Spetzler, Defect microdynamics and physical mechanisms of seismic wave attenuation and velocity dispersion in the Earth's mantle, Rev. Geophys. 28 (1990) 399–421.
[33] S. Karato, Mapping water content in the upper mantle, in: J. Eiler (Ed.), Subduction Factory, AGU Monograph, Washington, DC, 2001, in press.
[34] A.M. Dziewonski, D.L. Anderson, Preliminary reference earth model, Phys. Earth Planet. Inter. 25 (1981) 297–356.
[35] C.P. Conrad, B.H. Hager, Mantle convection with strong subduction zones, Geophys. J. Int. 144 (2001) 271–288.
[36] C.J. Hawkesworth, S.P. Turner, F. McDermott, D.W. Peate, P. van Calsteren, U–Th isotopes in arc magmas: implications for element transfer from the subducted crust, Science 276 (1997) 551–555.
[37] S.M. Peacock, K. Wang, Seismic consequences of warm versus cool subduction metamorphism: examples from Southwest and Northeast Japan, Science 286 (1999) 937–939.
[38] J.H. Davies, D.J. Stevenson, Physical model of source region of subduction zone volcanics, J. Geophys. Res. 97 (1992) 2037–2070.
[39] D.W. Scholl, R.H. Herzer, Geology and Resource Potential of the Southern Tonga Platform, in: J.S. Watkins, F. Shiqiang, K.J. McMillen (Eds.), Geology and Geophysics of Continental Margins, AAPG Mem. 53 (1992) 139–156.
[40] I. Moxon, Subsidence history of Great Valley: forearc basin evolution during Laramide Orogeny, Am. Assoc. Petrol. Geol. Bull. 70 (1986) 473–474.
[41] D.T. Sandwell, W.H.F. Smith, Marine gravity anomaly from GeoSat and ERS1 satellite altimetry, J. Geophys. Res. 102 (B5) (1997) 10039–10054.
[42] W.H.F. Smith, D.T. Sandwell, Global sea floor topography from satellite altimetry and ship depth soundings, Science 277 (1997) 1956–1962.
[43] F.G. Lemoine, S.C. Kenyon, J.K. Factor, R.G. Trimmer, N.K. Pavlis et al., The Development of the Joint NASA GSFC and NIMA Geopotential Model EGM96, Technical report, NASA Goddard Space Flight Center, Greenbelt, MD, 1998.